ACS APPLIED MATERIALS & INTERFACES

www.acsami.org

Research Article

Unlocking Wearable Microbial Fuel Cells for Advanced Wound Infection Treatment

Maryam Rezaie, Zahra Rafiee, and Seokheun Choi*

Cite This: *ACS Appl. Mater. Interfaces* 2024, 16, 36117−36130

Read Online

ACCESS | Metrics & More | Article Recommendations | Supporting Information

ABSTRACT: Better infection control will accelerate wound healing and alleviate associated healthcare burdens. Traditional antibacterial dressings often inadequately control infections, inadvertently promoting antibacterial resistance. Our research unveils a novel, dual-functional living dressing that autonomously generates antibacterial agents and delivers electrical stimulation, harnessing the power of spore-forming *Bacillus subtilis*. This dressing is built on an innovative wearable microbial fuel cell (MFC) framework, using *B. subtilis* endospores as a powerful, dormant biocatalyst. The endospores are resilient, reactivating in nutrient-rich wound exudate to produce electricity and antibacterial compounds. The combination allows *B. subtilis* to outcompete pathogens for food and other resources, thus fighting infections. The strategy is enhanced by the extracellular synthesis of tin oxide and copper oxide nanoparticles on the endospore surface, boosting antibacterial action, and electrical stimulation. Moreover, the MFC framework introduces a pioneering dressing design featuring a conductive hydrogel embedded within a paper-based substrate. The arrangement ensures cell stability and sustains a healing-friendly moist environment. Our approach has proven very effective against three key pathogens in biofilms: *Pseudomonas aeruginosa*, *Escherichia coli*, and *Staphylococcus aureus* demonstrating exceptional capabilities in both in vitro and ex vivo models. Our innovation marks a significant leap forward in wearable MFC-based wound care, offering a potent solution for treating infected wounds.

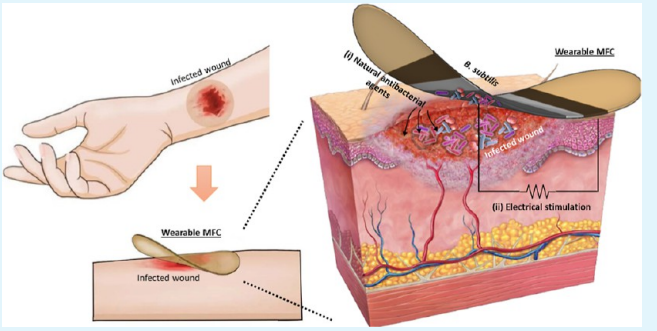

KEYWORDS: *infected wounds, wearable microbial fuel cells, antibacterial agents, electrical stimulation, Bacillus subtilis*

1. INTRODUCTION

Skin wounds undermine the structural integrity and physiological operations of cutaneous tissue, presenting formidable obstacles to the body's intrinsic reparative mechanisms.[1,2] The skin harbors diverse microbial communities that play a pivotal role in bolstering local and systemic immune defenses.[3,4] Intricate interactions with host epithelial and immune cells thwart the encroachment of pathogenic microorganisms.[5] However, compromised skin integrity from injury disrupts those immune functions.[6] Consequently, throughout wound healing, an environment rich in nutrients, moisture, and warmth develops, providing the perfect conditions for pathogens to invade and multiply.[7,8] This complicates wound care, making it more challenging to manage effectively. In infected wounds, the predominant bacterial strains frequently identified are the Gram-negative species *Pseudomonas aeruginosa* and *Escherichia coli*, alongside the Gram-positive species *Staphylococcus aureus*.[9,10] The progression of wound infection follows a continuum, initiating with "contamination," evolving into "colonization," and subsequently advancing to "local infection" as pathogens penetrate deeper into the wound tissue.[9] This progression is exacerbated as pathogens organize into biofilms, transitioning the infection from a localized issue to a "spreading infection" phase, ultimately culminating in the most critical stage, "systemic infection," which can lead to sepsis and organ dysfunction.[10] Biofilm formation poses a significant challenge because the film protects pathogens as they secrete extracellular polymeric substances.[11] The substances form a mechanical and chemical barrier, rendering the biofilm less susceptible to eradication by the human immune defense mechanisms.[12]

The traditional methodology for managing infected wounds primarily relies on embedding antibacterial agents into wound dressings.[13,14] This approach is designed to thwart the initial stages of pathogenic invasion or to completely eradicate pathogens from the wound. However, the indiscriminate or incorrect use of empirical antibacterial drugs has led to the emergence and spread of antibacterial resistance, simultaneously impairing the growth of beneficial microbial

Received: April 17, 2024
Revised: June 21, 2024
Accepted: June 24, 2024
Published: July 1, 2024

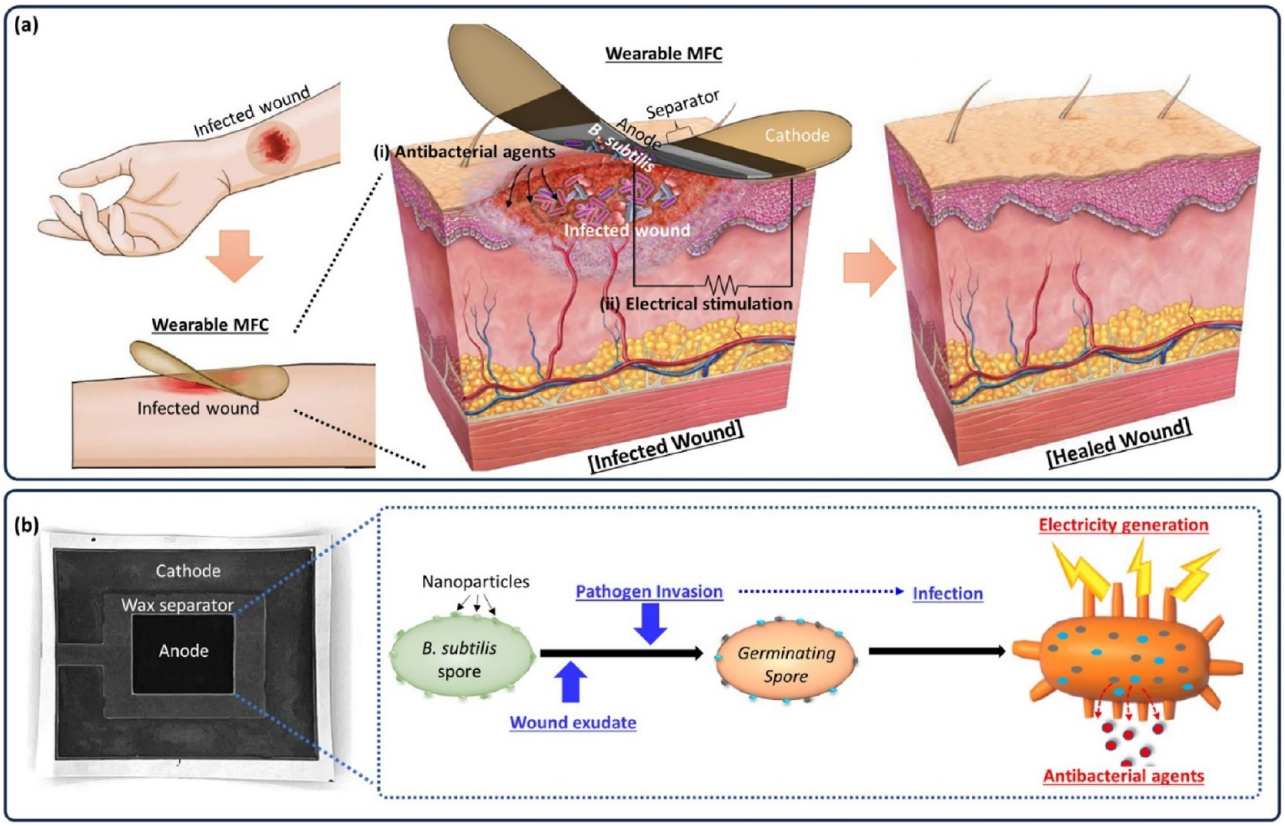

Figure 1. Enhanced MFC as a revolutionary wound-dressing solution. (a) Dual-functional living dressing to actively combat wound infections. It uniquely integrates the capability to autonomously generate antibacterial substances with the application of controlled electrical stimulation directly to the wound site. (b) Photo of the advanced MFC including spore-forming *Bacillus subtilis*. These resilient endospores are engineered to remain in a dormant state during prolonged storage, ensuring the longevity and efficacy of the dressing. Upon application to a wound, the presence of nutrient-rich exudate triggers these spores to emerge from dormancy, transitioning into an active metabolic state. This activation initiates a dual process where the bacteria begin to generate electricity extracellularly through their metabolic activities. Simultaneously, these activated cells produce and secrete antibacterial agents.

communities.[14] This disrupts the intricate balance of the skin's microbial ecosystem, essential for bolstering the human immune system and wound healing.[15] Consequently, the efficacy of traditional wound treatment strategies, aimed at the prevention and management of a broadening spectrum of wound infections, is significantly undermined. Moreover, the inherent limitations in preloading dressings with sufficient antibiotics necessitate their frequent replacement, which can interfere with natural wound healing and reduce the effectiveness of the treatment.[16] Even more concerning, biofilm formation can substantially enhance bacterial resistance to antibiotics, leading to more severe infections and diminishing the efficacy of antibacterial-laden dressings.[11,12] This escalation in pathogen resistance presents a significant challenge to existing wound care practices. The situation calls for a reevaluation of current antibacterial usage in wound care and for innovative research into novel treatment modalities that can effectively address these complex challenges.

Engineered living wound dressings embedded with probiotic microorganisms that produce natural antibacterial agents represent a promising advancement.[17,18] Those innovative dressings effectively inhibit pathogen growth while preserving beneficial microbial communities, offering a targeted approach to wound treatment. Unlike traditional dressings, an active living system continuously generates antibacterial compounds, eliminating the need for frequent replacements. The dressings use a hydrogel base with three-dimensional (3D) molecular networks, preventing the escape of probiotic bacteria into the surrounding skin and potentially causing further infections.[18] Their porous yet breathable structure maintains a moist and oxygen-enriched environment, crucial for the survival of the probiotic bacteria and the healing of wounds. Additionally, the superior biocompatibility of the hydrogel and the probiotic bacteria significantly reduces the risk of immune system reactions, thereby sustaining the therapeutic effectiveness and bacterial viability in wound management.[18,19] Previously, innovative hydrogel dressings encapsulating living *Lactobacillus* have been developed to eliminate harmful bacterial infections, thereby accelerating wound healing.[20] In another advancement, hydrogel dressings loaded with living *Lactococcus* have been engineered to regulate therapeutic angiogenesis, significantly enhancing the healing of diabetic wounds.[18] In another work, hydrogels incorporated with *Bacillus subtilis* have been designed to continuously produce antifungal agents, offering a proactive approach to combating fungal infections.[21] Enhanced synergistic collaboration between *Chlorella* and *B. subtilis* has been leveraged to expedite wound healing.[22] *Chlorella* generates oxygen that alleviates hypoxia and fosters the proliferation of *B. subtilis*. In turn, *B. subtilis* synthesizes antibacterial agents, effectively targeting and eradicating pathogens. The potential of leveraging bioengineered living hydrogels presents significant opportunities for innovative wound dressing platforms, yet this arena remains nascent with several pivotal challenges to overcome for practical application.

https://doi.org/10.1021/acsami.4c06303
ACS Appl. Mater. Interfaces 2024, 16, 36117−36130

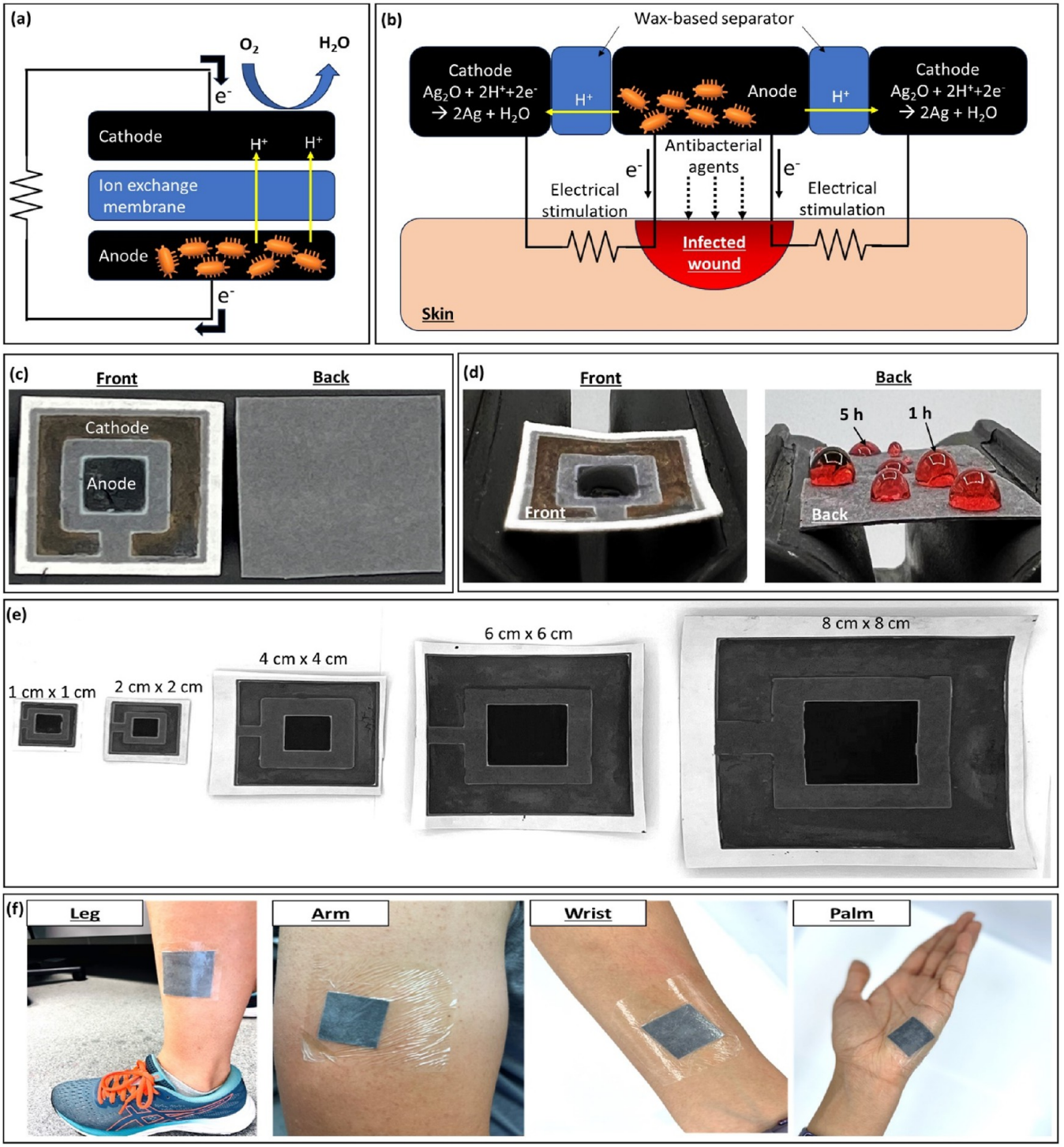

Figure 2. Enhanced designs and functionalities of MFC-based wound dressings. (a) Traditional vertical configuration of MFCs. (b) An advanced horizontal configuration designed to improve wound healing. This structure actively secretes antibacterial agents and delivers electrical stimulation to the wound site, targeting effective infection control and enhanced healing processes. (c) Photographs of the fully assembled MFC, showcasing the practical assembly and design aesthetics of the wound dressing. (d) The interaction of liquid droplets with the MFC's surface. When introduced to the anode side, droplets are instantly absorbed, demonstrating efficient fluid management. Conversely, droplets remain unabsorbed on the hydrophobic back side, indicating selective material properties that prevent unwanted moisture penetration. (e) The adaptability of the MFC design to various scales, highlighting the potential for customization and application across different wound sizes and types. (f) The flexibility and comfort of wearing the MFC dressing on various body parts, emphasizing its suitability and adaptability for long-term wear in diverse anatomical locations, thereby ensuring continuous wound monitoring and treatment.

Primarily, the long-term storage of hydrogels preloaded with microorganisms poses a substantial hurdle, as these bacteria-infused dressings demand ongoing maintenance to preserve microbial viability until deployment. Furthermore, integrating living microorganisms within polymeric hydrogels often necessitates conditions detrimental to their survival, such as

https://doi.org/10.1021/acsami.4c06303
ACS Appl. Mater. Interfaces 2024, 16, 36117−36130

high temperatures, pressure, and the employment of toxic chemicals during fabrication, all of which can significantly impair their viability or result in their demise. Additionally, the limited quantity of antibacterial agents produced by the preloaded microorganisms proves to be insufficient in combating severe pathogenic invasions or in eliminating well-established pathogenic biofilms. Therefore, relying solely on a singular therapeutic approach will not provide a reliable treatment for infected wounds, underscoring the need for multifaceted strategies.

In this report, we introduce a dual-functional living dressing capable of autonomously producing antibacterial agents and delivering controlled electrical stimulation, using spore-forming *Bacillus subtilis* (Figure 1a). The dressing was engineered around a two-dimensional advanced microbial fuel cell (MFC) architecture, incorporating *B. subtilis* endospores as a dormant yet potent biocatalyst. Remarkably, these endospores can withstand extended storage in dormancy and become metabolically active upon exposure to nutrient-rich wound exudate that permeates the dressing. Upon activation, the germinated cells commence extracellular electricity generation via metabolic processes while secreting antibacterial agents to outcompete pathogens for scarce resources, thus ensuring their survival (Figure 1b). The dual-therapeutic strategy demonstrated a profound antibacterial effect, capable of eradicating biofilms produced—or even preventing their formation—by the pathogens *P. aeruginosa*, *E. coli*, and *S. aureus*. The enhancement of antibacterial efficacy and electrical output for stimulation was achieved through the extracellular biosynthesis of tin oxide (SnO_2) and copper oxide (CuO) nanoparticles on the surface of the endospores. These nanoparticles, known for their inherent antibacterial properties, have been used extensively in treating infected wounds.[23] Moreover, they can facilitate electronic or electrochemical connections between the cells and an external electrode, significantly boosting electricity generation.[24,25] Importantly, these biogenically produced nanoparticles are biocompatible with human skin.[26] Furthermore, we present a pioneering design for wound dressings that incorporates a conductive hydrogel within a paper-based substrate. This unique configuration secures the cells within its framework and maintains an optimal moisture-rich environment, fostering effective wound healing. In vitro and ex vivo experiments demonstrated remarkable resistance against pathogenic biofilms, underscoring the potential of this strategy. Consequently, we believe that the approach delineated herein heralds a new paradigm in wearable MFC-based wound dressings, offering enhanced effectiveness in the treatment of infected wounds.

2. RESULTS AND DISCUSSION

2.1. Wearable MFC-Based Wound Dressings. An MFC is a bioelectrochemical system that harnesses the metabolic processes of electricity-generating bacteria to convert chemical energy directly into electrical energy.[27,28] Traditionally, MFC technology was focused primarily on macroscale applications, including power generation and wastewater treatment.[29,30] However, technological limitations and too-slow progress led to skepticism among researchers regarding the feasibility of large-scale applications.[31−33] Concurrently, the miniaturization of MFC technology has emerged as a compelling area of research, garnering significant interest for its potential as an innovative and efficient energy harvester in portable, low-power applications.[34,35] Numerous miniature MFCs have been developed, offering promising on-demand power sources for portable electronics, robotic devices, and Internet of Things applications.[36−39] Notably, advancements have even enabled small-scale MFCs to operate using human-derived microorganisms and bodily fluids as fuel sources.[40−43] Our research group has pioneered the development of wearable MFCs that harness skin microorganisms, demonstrating their capability to generate sufficient energy for electronic devices and biosensors.[43] Specifically, we were the first to use spore-forming *B. subtilis* as an electricity-producing biocatalyst and achieved continuous and long-term power generation through cycles of germination and sporulation, triggered by the availability of nutritious sweat on human skin.[44−46] In this study, we extend the potential applications of wearable MFC technology by investigating its feasibility as a dressing designed specifically for the treatment of infected wounds. This marks the first exploration into using wearable MFC technology for this purpose. Our comprehensive review of the existing literature revealed that *B. subtilis* secretes significant quantities of antibacterial agents that inhibit the growth of competing pathogens.[21,22,47,48] Experimental evidence confirms that *B. subtilis* can effectively balance antibacterial production and growth when in competition with pathogens.[49,50] Additionally, electrical stimulation has been shown to exert an inhibitory effect on pathogen proliferation.[51,52] Moreover, evidence suggests that direct current at the microampere level is particularly effective in inhibiting bacterial growth.[53]

We hypothesize that an MFC preloaded with *B. subtilis* can serve as a pioneering and dynamic solution for the treatment of infected wounds. In the conventional design of MFCs, the architecture is predominantly vertical, comprising two electrodes separated by an ion exchange membrane (Figure 2a). The anode harbors electricity-producing biocatalysts that decompose organic materials, thereby releasing electrons and protons. Electrons traverse to the cathode via an external circuit, whereas protons move internally through the ion exchange membrane to reach the cathode. At the cathode, a reduction reaction occurs, facilitated by the recombination of electrons and protons. In our study, we enhanced the traditional MFC design by introducing a novel horizontal configuration (Figure 2b). This layout precisely positioned the anode directly above the wound bed, while the cathode was horizontally arranged to encircle the anode (Figure 2c). Enhancements to this configuration were achieved by incorporating a wax-patterned separator that serves as the ion exchange membrane,[54,55] positioned effectively between the anode and cathode. The design leverages the inherent electrically resistive qualities of human skin,[56] employing it as the external circuit that links the anode, positioned directly on the infected wound, to the cathode, situated on healthy skin (Figure 2b). Such an innovative arrangement facilitates the precise administration of antibacterial agents and electrical stimulation directly to the infected area. This method promises to substantially enhance the treatment's efficacy, providing a focused strategy for wound management.

The device was developed on a paper substrate by precisely patterning hydrophobic wax areas and introducing functional inks to the defined hydrophilic regions. The wax acted as an effective membrane for ionic transfers and electrically separating the anode from the cathode. Our group pioneered many paper-based MFCs,[54,55] which were leveraged specially for wound dressing here. The hydrophilic anodic area that will directly contact the wound bed absorbs the simulated wound

https://doi.org/10.1021/acsami.4c06303
ACS Appl. Mater. Interfaces 2024, 16, 36117−36130

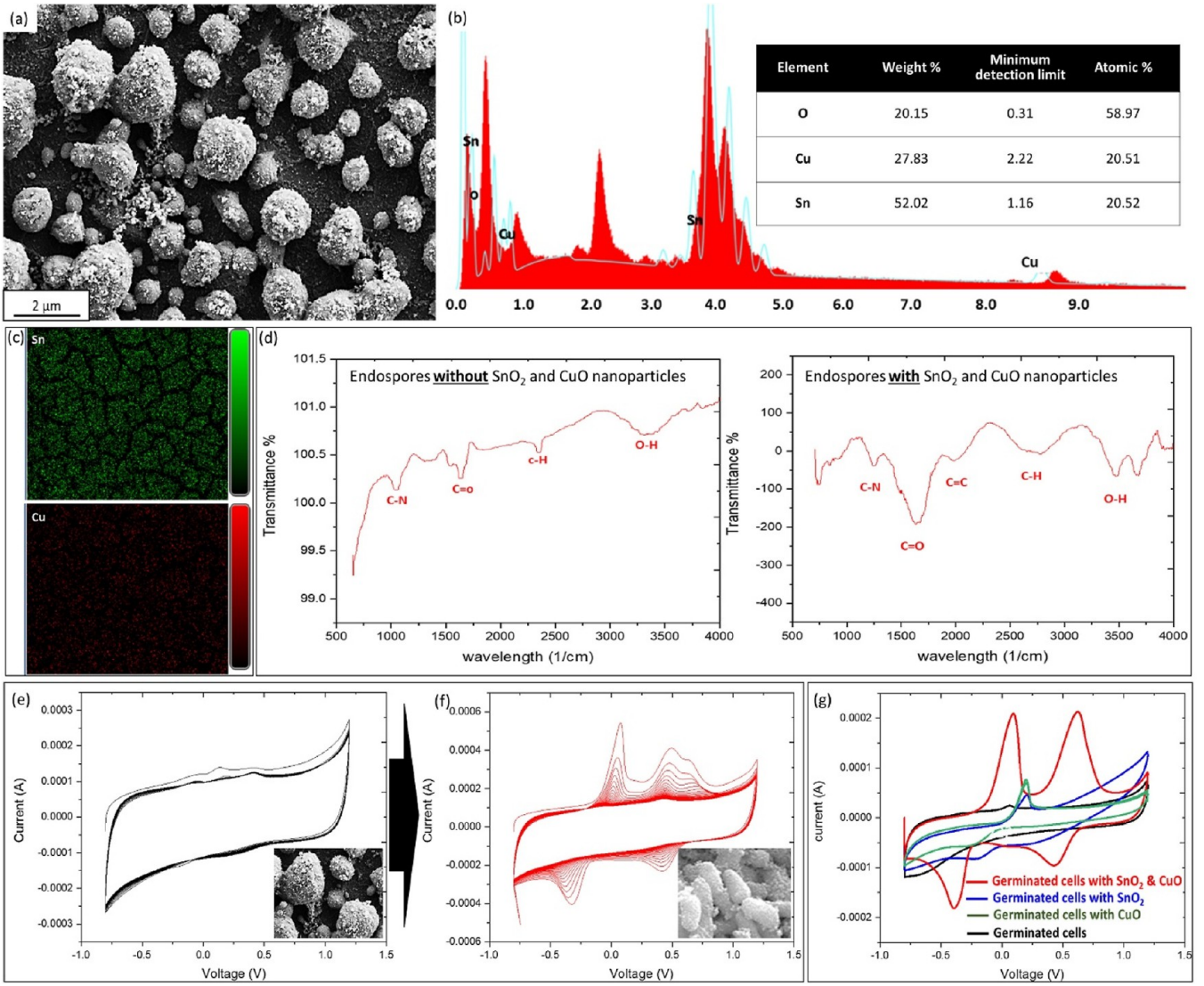

Figure 3. Detailed characterization of *B. subtilis* endospores encapsulated with biosynthesized nanoparticles. (a) Scanning electron microscopy (SEM) image showcasing the surface morphology. (b) An energy dispersive X-ray (EDX) spectrum for elemental analysis. (c) EDX elemental mapping highlighting the distribution of O, Cu, and Sn. (d) FTIR spectra comparing samples with and without nanoparticles. The first 20 cycles of cyclic voltammetry (CV) profiles of the nanoparticle-decorated (e) endospores and (f) germinated cells. (g) CV profiles of the germinated cells decorated with and without various nanoparticles.

exudate instantly while the hydrophobic backside of the MFC repels potential moisture and bacterial invasion from the environment (Figure 2d). The horizontal MFC is easily adaptable to various scales, highlighting the potential for customization and application across different wound sizes and types (Figure 2e). Furthermore, the flexibility and comfort of wearing the MFC dressing on various body parts emphasizes its suitability and adaptability for long-term wear in diverse anatomical locations, thereby ensuring continuous wound monitoring and treatment (Figure 2f).

2.2. Revolutionizing the MFC. The efficacy of the proposed wound dressing was substantially enhanced through two distinct strategies. The first involves the extracellular integration of specific nanoparticles onto the surface of endospores. The integration strengthens the antibacterial properties of the dressing, while simultaneously boosting its electrical current and power output. Such dual functionality targets infection control and enhances bioelectric applications. The second strategy employs a composite hydrogel matrix embedded within a paper-based substrate. That design promotes bacterial adhesion and sustains a moisture-rich environment conducive to healing. Additionally, it protects the encapsulated bacteria from external threats. Together, these strategies create a symbiotic protective ecosystem within the dressing, optimizing wound recovery and care. This holistic approach leverages advanced materials science and biotechnology to address critical aspects of wound management, including antibacterial defense, bioelectrical stimulation, and environmental regulation, offering a comprehensive solution to enhance healing processes. Guided by our central hypothesis outlined in Section 2.1 and informed by these strategic advancements, our goal is to meticulously design an advanced MFC that is specifically optimized for application as an active wound dressing.

B. subtilis is typically characterized as a bacterium with limited electrogenic capabilities, attributed largely to its thick, insulating outer cell membrane.[44] Furthermore, the antibacterial efficacy of *B. subtilis*, achieved through the production of

https://doi.org/10.1021/acsami.4c06303
ACS Appl. Mater. Interfaces 2024, 16, 36117−36130

antibiotic agents, necessitates significant enhancement to effectively combat severe pathogenic invasions and to eradicate well-established pathogenic biofilms. Previous studies have demonstrated that nanoparticles biosynthesized by cells can significantly enhance the current and power output of MFCs.[24,25] Separately, nonbiologically synthesized SnO_2 and CuO nanoparticles have been explored as alternative antibacterial agents to address the growing issue of antibiotic resistance.[23] In this study, we propose a novel approach by employing extracellularly biosynthesized SnO_2 and CuO nanoparticles on *B. subtilis*. Upon exposure of vegetative *B. subtilis* cells to a solution containing tin(II) chloride ($SnCl_2$) and copper(II) chloride ($CuCl_2$), the positively charged ions Sn^{2+} and Cu^{2+} were attracted to the negatively charged bacterial cell wall. This interaction initiated an electrochemical activity within the bacteria, leading to the biosynthesis of SnO_2 and CuO nanoparticles through oxidation.[25] Remarkably, in response to the high concentrations of these potentially toxic metal ions, the vegetative cells underwent sporulation, forming endospores as a survival and adaptation strategy.[57] This process allowed the newly formed nanoparticles to bind to the protective outer layers of the endospores. SEM analysis revealed the formation of nanoparticles of varied sizes on the surface of the endospores (Figure 3a). Complementary EDX microanalysis detected the elemental signatures of tin (Sn), copper (Cu), and oxygen (O), confirming the successful synthesis of SnO_2 and CuO nanoparticles (Figure 3b). EDX mapping demonstrated a widespread distribution of Sn and Cu elements across the samples, indicating a uniform nanoparticle coating (Figure 3c). Fourier-transform infrared spectroscopy (FTIR) was employed to compare the spectroscopic profiles of endospores before and after nanoparticle synthesis (Figure 3d). Notable observations included a significant increase in transmittance percentage and peak intensities in the spectra of nanoparticle-decorated *B. subtilis* spores. This indicates surface modifications and interactions between the nanoparticles and spore surfaces, which may alter the infrared absorption properties of the spores, enhancing spectral features and peak intensities. Such interactions could potentially dilute the sample or reduce its thickness, further contributing to the observed increase in transmittance. The FTIR spectra highlighted key features associated with lipid vibrations, specifically the stretching vibrations of C−H bonds in the 2800−3000-cm^{-1} range and the stretching vibrations of ester carbonyl (C═O) bonds in the 1740−1750-cm^{-1} range, underscoring the biochemical changes induced by nanoparticle synthesis. The FTIR spectrum analysis revealed notable changes postsynthesis, including shifts in peak positions and variations in peak intensity. Specifically, the peaks corresponding to functional groups C−N, C═O, C−H, and O−H exhibited shifts to higher wavenumbers, indicative of their involvement in the binding mechanism with the nanoparticles. Additionally, new peaks emerged at 2000 and 3700 cm^{-1}, representing the C═C bonds and the nanoparticles, respectively. These spectral changes underscore the chemical interactions during the nanoparticle synthesis process. The initial 20 cycles of the CV profile consistently demonstrated stable and unchanged electrochemical behavior for the nanoparticle-enhanced endospores (Figure 3e). This stability is crucial for the application of wound dressings, ensuring their functionality is maintained over long storage periods in a dormant state. *B. subtilis* endospores, in their dormant phase, exhibit negligible redox peaks in CV measurements due to their metabolically inactive state, which results in minimal redox activity. However, upon exposure to a nutrient-rich simulated wound exudate, simulating conditions of a healing wound, the endospores transition to a metabolically active state. This transition triggers significant electrochemical activity, as evidenced by increasing redox activity in the CV profile over the initial 20 cycles (Figure 3f). The nanoparticles adhering to the spore surface are crucial, acting as both electron transfer facilitators and catalysts for redox reactions, markedly enhancing the efficiency of electron transfer processes and catalytic activities (Figure 3g). This synergy between the endospores and nanoparticles is instrumental in generating a reduction peak in the CV curves postgermination. Notably, the electrochemical activity was markedly enhanced in cells simultaneously adorned with SnO_2 and CuO nanoparticles (Figure 3g). Comparatively, cells coated solely with SnO_2 or CuO exhibited less pronounced electrochemical activities, though still superior to cells without nanoparticle enhancement. This indicates the synergistic effect of combining SnO_2 and CuO nanoparticles on the electrochemical performance of the endospores.

The synergistic integration of nanoparticles exhibited enhanced antibacterial properties against three key pathogenic biofilms: *P. aeruginosa*, *E. coli*, and *S. aureus*. This was determined through disc diffusion assays, which assessed the susceptibility of these pathogens to native *B. subtilis* and its nanoparticle-augmented variants. *B. subtilis* inherently possesses antibacterial capabilities, attributed to its production of antibiotic compounds. *Bacillus* species are renowned for their ability to produce a variety of antibiotics, including penicillin, streptomycin, and erythromycin. Additionally, research has confirmed that *B. subtilis* secretes fengycins, which effectively eliminate *S. aureus* by inhibiting its quorum sensing mechanisms.[22] However, the presence of both types of nanoparticles on *B. subtilis* significantly lengthened the inhibition zone diameters around the treated discs, as observed in the assays (Figure S1). This amplification indicates that the nanoparticle combination notably improves the antibacterial efficacy of *B. subtilis*, suggesting a potentiated therapeutic potential for treating infections in wound care. Our strategy with nanoparticles served dual purposes: first, to act as an electrical conduit, facilitating a marked improvement in the rate of electron transfer across the cell membrane, and second, to function as an innovative nanomaterial-based therapeutic strategy against bacterial infections. Through this dual-functionality approach, we anticipate enhancing the electrical production capabilities of *B. subtilis* in MFC applications and offering a promising avenue for the development of novel antibacterial therapies.

The elaboration of the second strategic approach for our advanced wound dressing design is presented. Paper-based devices have garnered widespread application in the realms of bacterial detection and therapeutic interventions, attributed to their cost-effectiveness, inherent flexibility, disposability, and ease of modification.[8,58] Beyond these practical advantages, paper-based platforms bring forth several distinct benefits for wound dressing applications compared to traditional methods.[59] These include superior biocompatibility, hypoallergenic properties, and a hygroscopic, breathable structure. Such characteristics are indispensable for fostering wound healing, facilitating oxygen exchange, and maintaining optimal moisture levels at the wound site. Nonetheless, embedding living *B. subtilis* cells into a nonconductive paper substrate to create an

https://doi.org/10.1021/acsami.4c06303
ACS Appl. Mater. Interfaces 2024, 16, 36117−36130

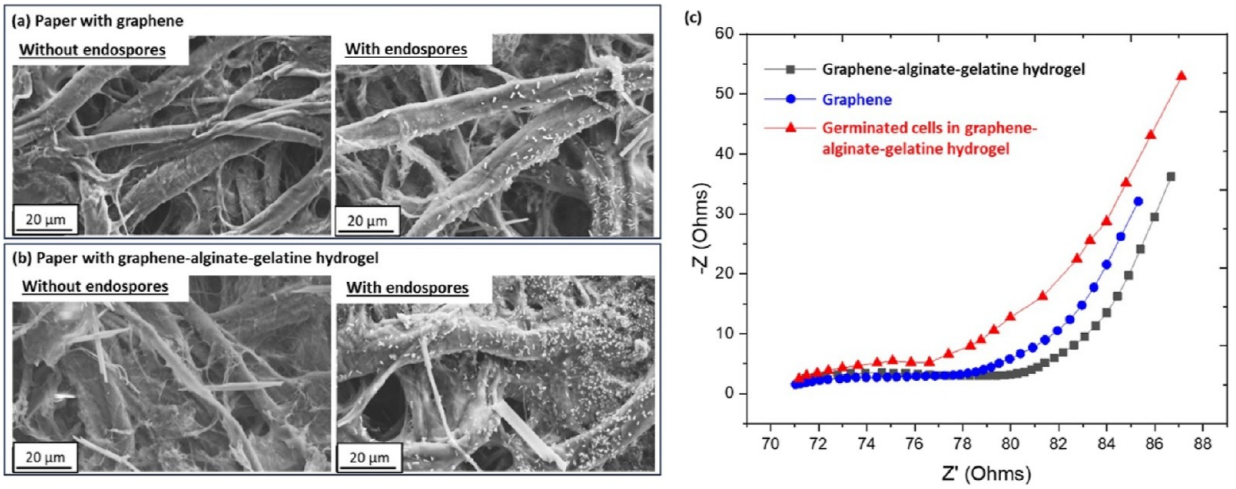

Figure 4. SEM images of (a) the substrate without the addition of sodium alginate and gelatin, serving as a control, and (b) the substrate with the incorporation of sodium alginate and gelatin. (c) Electrochemical impedance spectroscopy (EIS) profiles for these samples.

MFC-integrated wound dressing presents considerable challenges. This innovative approach requires attracting a significant quantity of bacterial cells and preserving their viability during the fabrication. A critical hurdle is engineering the dressing to incorporate physical barriers that prevent the *B. subtilis* cells from contaminating the wound bed, while simultaneously ensuring the material remains breathable and porous enough to support oxygen and moisture exchange essential for healing. Addressing these challenges is crucial for the successful development of a paper-based, MFC-functional wound dressing that leverages the unique properties of *B. subtilis* for enhanced wound care. Here, we introduce an innovative wound dressing design consisting of a conductive hydrogel-infused paper-based substrate. The hydrogel, characterized by its great bioaffinity, effectively attracts and retains a significant number of *B. subtilis* cells within its tightly knit 3D molecular network, ensuring the cells are securely housed within the structure (Figure S2). Concurrently, the paper component acts as a robust yet flexible mechanical scaffold, facilitating the incorporation of various essential components for MFC functionality. This hybrid design allows the use of dormant *B. subtilis* endospores, which transform during nanoparticle synthesis, serving as a resilient biocomponent capable of withstanding harsh fabrication conditions without compromising cell viability. The conductive hydrogel, synthesized via a hydrothermal method, comprised graphene, sodium alginate, and gelatin. Sodium alginate (a natural polysaccharide derived from seaweed) and gelatin (a protein obtained from collagen) augment the biocompatibility, bioaffinity, and moisture retention of the dressing. The gel was combined with poly(3,4-ethylenedioxythiophene):polystyrenesulfonate (PEDOT:PSS) to form the anodic material. Nanoparticle-enhanced endospores were integrated into the anodic mixture, which was then strategically embedded within predefined regions of the paper substrate. Microscopic analysis, as demonstrated in Figure 4a,b, reveals that the addition of sodium alginate and gelatin to the anodic material did not significantly alter the morphological integrity of the paper's fibrous network. However, a substantial increase in the presence of *B. subtilis* cells is observed within the areas treated with the composite hydrogel. EIS analysis indicates that the incorporation of the composite hydrogel alongside the germinated cells markedly enhances electron transfer efficiency during metabolic activity, despite the inherent increase in interfacial resistance attributed to the insulating nature of the hydrogel's polymeric constituents (Figure 4c).

The *B. subtilis* cells, upon germination and subsequent decoration with SnO_2 and CuO nanoparticles embedded within a composite hydrogel, exhibited pronounced antibacterial properties against the pathogens *E. coli*, *P. aeruginosa*, and *S. aureus* (Figure S3). Notably, in the presence of the hydrogel alone, there was a continuous and marked increase in the concentration of these pathogens. Conversely, the endospores decorated with nanoparticles within the hydrogel matrix led to a significant reduction in pathogen proliferation, even in the absence of germination, highlighting the powerful antibacterial effects exerted by the nanoparticles. Further investigation into the antibacterial efficacy of these nanoparticles was conducted by isolating the biosynthesized SnO_2 and CuO nanoparticles from the cells and exposing them directly to the pathogens. This approach yielded substantial antibacterial activity, reinforcing the potential of these nanoparticles as effective antibacterial agents. The most compelling results were observed with the germinated cells, suggesting that the antibacterial activity was not solely attributable to the intrinsic antibacterial properties of the nanoparticles but was significantly enhanced by the production of antibacterial agents by the cells themselves. This synergy between the biological and nanoparticle components underscores the innovative potential of this approach for enhancing antibacterial efficacy.

In paper-based wound dressings, moisture management is crucial, involving efficient water absorption and retention. An effective dressing should simultaneously absorb excess moisture, showcasing hydrophilicity, and maintain optimal moisture to support healing, demonstrating water retention.[60] Controlled swelling is vital, as it ensures a moist wound environment and allows the dressing to conform to wound contours. Our research indicates that our composite hydrogel outperforms standard controls in moisture management because of its 3D structure of sodium alginate and gelatin, which increases surface area and swelling (Figure S4). Unlike pure graphene, which is dense and less absorbent, our hydrogel blend creates a porous network that effectively traps and holds water, enhancing swelling. This feature, absent in pure graphene, along with superior water retention in the composite

https://doi.org/10.1021/acsami.4c06303
ACS Appl. Mater. Interfaces 2024, 16, 36117−36130

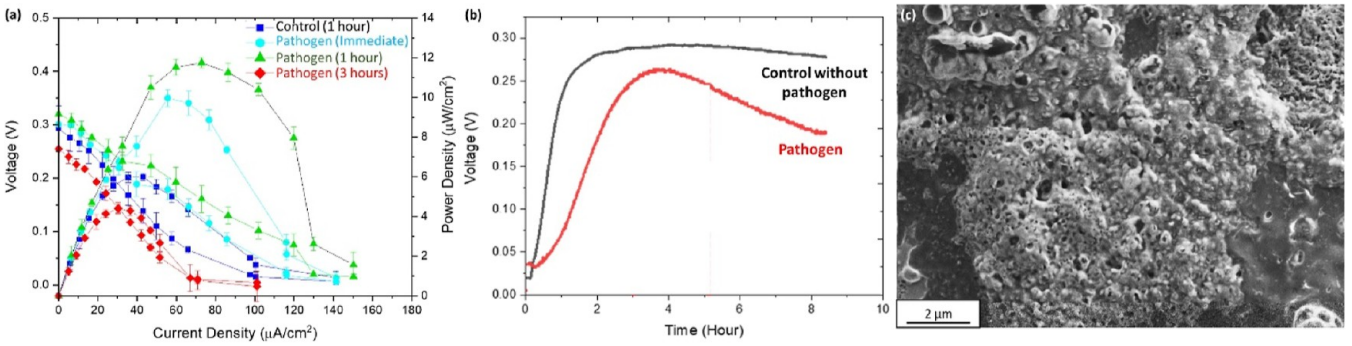

Figure 5. Assessment of the MFC performance in pathogen-rich environments. (a) Polarization curve and power output of the MFC when exposed to simulated wound exudate, comparing conditions with and without pathogens. (b) Real-time voltage output of the MFC, highlighting differences between operations in pathogen-free and pathogen-present environments. (c) SEM image of the pathogens taken 8 h after treatment with the MFC.

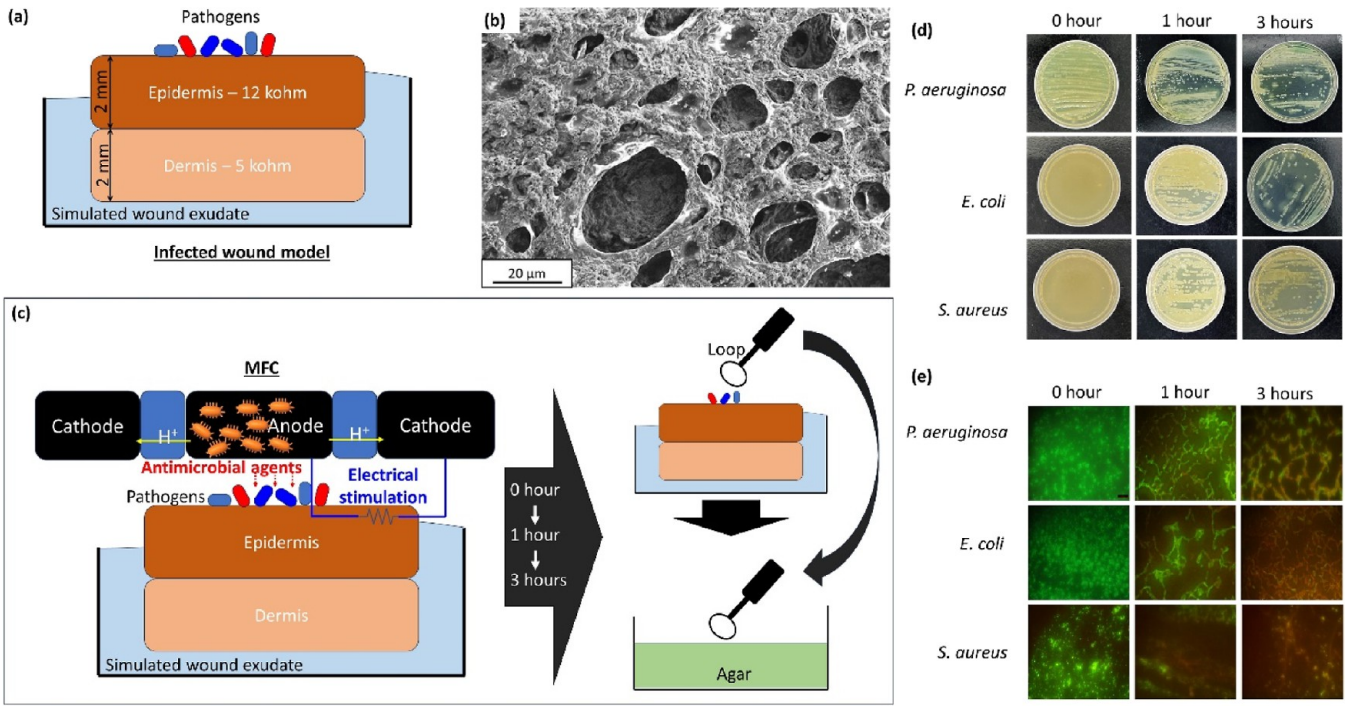

Figure 6. In vitro assessment of the MFC's antibacterial activity. (a) Diagram of the infected wound model. (b) SEM image of the synthetic skin. (c) Diagram of the in vitro testing procedures. (d) Photographs and (e) fluorescence microscopy images of the pathogens transferred on Petri dishes. Fluorescent microscopy differentiates between 5(6)-carboxyfluorescein diacetate (cFDA) in green and propidium iodide (PI) in red. cFDA renders live pathogens green, whereas PI stains dead cells red.

hydrogel, underlines the importance of sodium alginate and gelatin in improving moisture management and facilitating wound healing.

2.3. In Vitro and Ex Vivo Antibacterial Activity of the MFC. Before conducting in vitro and ex vivo assessments of the MFC, we scrutinized its performance in the presence of pathogens to understand its interaction dynamics. In this setup, the anodic compartment was inoculated with a mixture of three representative pathogenic bacteria (i.e., *P. aeruginosa*, *E. coli*, and *S. aureus*), each at a concentration corresponding to an optical density of 1.5 at 600 nm (OD_{600}), whereas the control condition involved only simulated wound exudate without pathogens. This experiment included pathogens such as *P. aeruginosa* and *S. aureus*, both known for their inherent ability to generate electricity.[61] Upon introduction of these bacteria, an immediate generation of electrical power was observed, which saw a gradual increase as the *B. subtilis* endospores began to germinate in response to the nutrient-rich simulated wound exudate (Figure 5a). Remarkably, the power output recorded at 1 h postpathogen introduction was significantly higher compared to the setup that included only the simulated wound exudate. However, beyond the 3-h mark, a pronounced decline in the MFC's electrical performance was noted, in stark contrast to the control setup, which maintained a stable performance for more than 8 h (Figure 5b). This decline is hypothesized to result from the combined antibacterial action of the nanoparticle-enhanced *B. subtilis* and its antibiotic production, which effectively inhibits the growth and metabolic activity of the introduced pathogens, leading to their subsequent elimination. The observed decrease in power output, dropping below control levels, suggests an accelerated depletion of nutrients (Figure 5a). Supporting this

https://doi.org/10.1021/acsami.4c06303
ACS Appl. Mater. Interfaces 2024, 16, 36117−36130

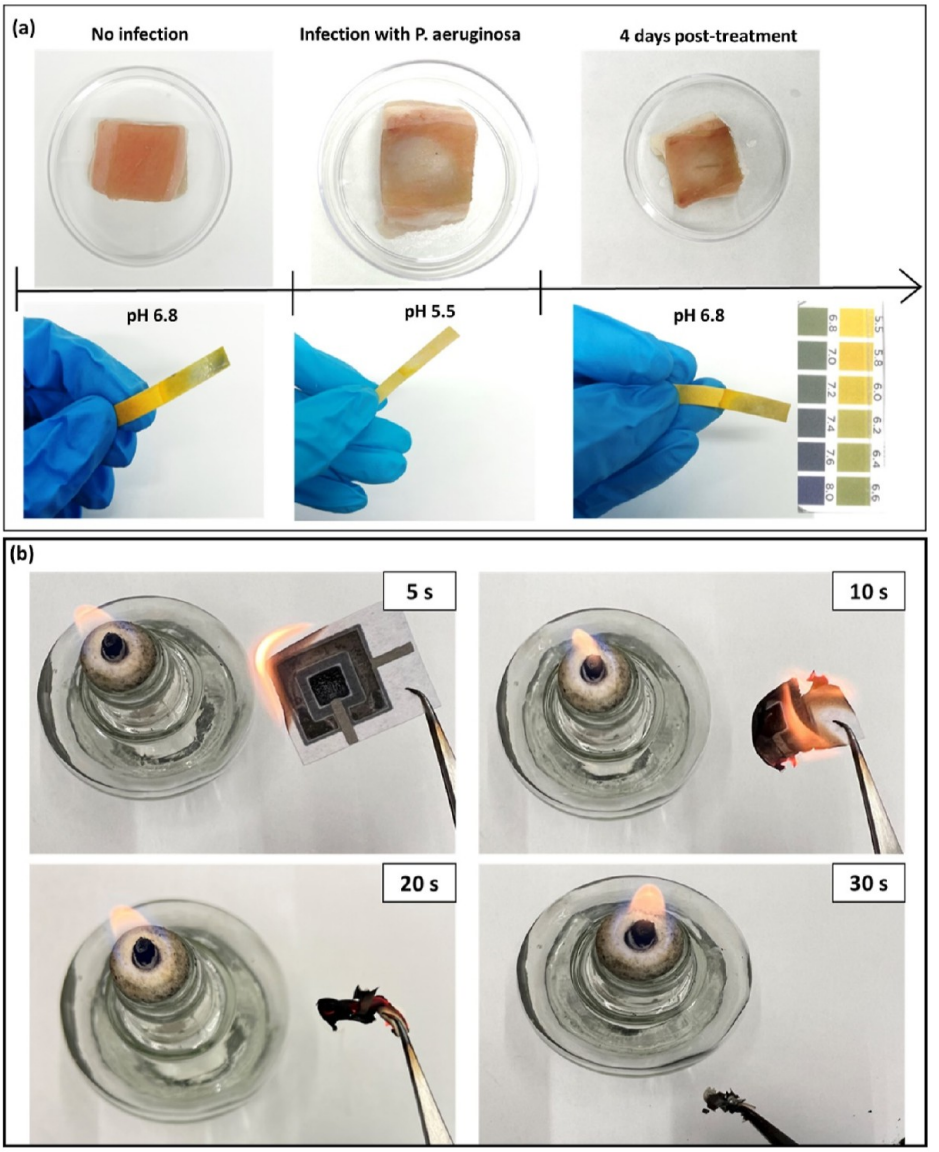

Figure 7. Ex vivo evaluation of the MFC-based wound dressing's antibacterial efficacy. (a) The quantification of pH levels on the surface of infected porcine skin models prior to and subsequent to the application of MFC treatment. (b) Disposal of the paper-based MFC wound dressing by incineration.

hypothesis, SEM images of the pathogens taken after 8 h of operation revealed significant damage to their cell membranes, confirming the antibacterial efficacy of the nanoparticle-decorated *B. subtilis* (Figures 5c and S5).

To rigorously assess the bifunctional antibacterial efficacy of the MFC, we devised an infected wound model using a synthetic conductive skin analog. This model integrates a bilayer structure, comprising a 2-mm-thick epidermis and a similarly thick dermis. Following exhaustive optimization through numerous iterations of material combinations (Figure S6a), we engineered a skin surrogate that closely replicates human skin's architecture and electrical properties.[56] We developed a novel conductive composite by infusing polypyrrole into an agar matrix with poly(vinyl alcohol) (PVA), enhanced with calcium chloride and sodium chloride. That enabled us to precisely achieve target resistivities of 12 kΩ for the epidermis and 5 kΩ for the dermis, as demonstrated in Figures 6a, S6b,c. This setup simulates the electrical characteristics of human skin and its intricate porous texture (Figure 6b). Subsequently, the artificial skin was placed in a Petri dish containing a fluid meant to simulate wound exudate. We inoculated specific pathogens onto localized areas of the epidermis, cultivating them for more than 24 h to replicate an infected wound. The MFC, featuring endospores adorned with SnO_2 and CuO nanoparticles, was then positioned over the infected site. The device's anode was aligned with the wound, whereas the cathode contacted the surrounding, uninfected tissue, establishing an electrical circuit through the epidermis that acted as an external resistor. At predetermined intervals (0, 1, and 3 h), samples from the pathogen-colonized region were collected using an inoculation loop and cultured on fresh agar plates (Figure 6c). We observed electrical current generation and antibacterial agent production by the MFC that began with the germination of endospores in the presence of the wound exudate. Over time, a significant reduction in the proliferation and growth of the cultured pathogens was noted, substantiating the MFC's potential as an effective antibacterial wound dressing (Figure 6d,e). Electrical stimulation has been

https://doi.org/10.1021/acsami.4c06303
ACS Appl. Mater. Interfaces 2024, 16, 36117−36130

demonstrated to damage the bacterial cell membrane, effectively reducing bacterial infection, as illustrated in Figure 5c. This technique has shown a direct antibacterial effect on both Gram-negative and Gram-positive bacteria in previous studies.[51−53] The use of a small current at low voltage results in high impedance, making it challenging for the electric current to pass through skin tissue. This characteristic makes electrical stimulation not only effective but also safe and straightforward to use.

In the development of our ex vivo skin infection model, porcine skin underwent preparation that included cleansing with phosphate-buffered saline (PBS) and subsequent sterilization using ethanol (Figure 7a). To simulate infection, a 4-mm diameter biopsy punch was employed to remove the top layer of the epidermis, which was then inoculated with *P. aeruginosa*. To facilitate biofilm formation, the inoculated skin samples were incubated for 24 h at 30 °C. Following the incubation, the MFC-based wound dressing was carefully applied to the affected area. To ensure a robust attachment of the MFC dressing to the porcine skin, transdermal adhesive tape was utilized. Throughout the experiment, 100 μL of simulated wound exudate were introduced to the wound site at 6 h intervals, mirroring the dynamic environment of a healing wound. *P. aeruginosa* is well-documented for its production of acidic metabolic byproducts throughout its growth phase. The presence of a *P. aeruginosa* infection in the tissue model led to localized acidification, a phenomenon that was quantitatively monitored through the use of pH-sensitive test paper.[62] Initially, the pH test paper transitioned from dark green, indicative of a neutral pH, to bright yellow, signaling acidification from the infection (Figure 7a). Remarkably, 4 days post-treatment with the MFC-based therapeutic intervention, the pH test paper reverted to dark green. This change signifies a return to neutral pH levels, suggesting the effective mitigation of the infection and the restoration of the tissue's normal pH balance.

A fundamental criterion for effective wound management materials is their safe and efficient disposability. Improper disposal of used dressings can lead to environmental contamination and increase the risk of propagating bacterial infections from the residual pathogens and microorganisms they harbor. In contrast to conventional wound dressings, which necessitate stringent disposal protocols, our innovative paper-based wound dressings offer straightforward and eco-friendly disposal through incineration. This method significantly minimizes the potential for environmental contamination and bacterial spread. The designed wound dressing demonstrates remarkable efficiency in this regard, requiring approximately 30 s to achieve complete combustion (Figure 7b). Such a feature enhances the practicality of using paper-based dressings in wound care.

3. FUTURE DIRECTION

This research provides a pivotal initial validation of the novel concept underlying the MFC-based wound dressing. The efficacy of this innovative approach as a wound dressing has been substantiated through rigorous in vitro and ex vivo investigations. However, to fully establish its therapeutic potential, the wound-healing capabilities of the MFC must be corroborated through in vivo studies employing bacteria-infected wound models. Additionally, there is a pressing need for comprehensive analysis to fully grasp the effect of MFC-generated electrical currents on the healing processes of infected wounds. This exploration should include determining the precise electrical current levels that enhance healing while maintaining tissue health and functionality. Although electrical stimulation has proven effective in treating infections, it also offers promising therapeutic benefits by promoting epithelialization, encouraging fibroblast migration, and enhancing vascularity, thus presenting significant opportunities in wound care management.[63] Additionally, while the antibacterial effects of compounds produced by *B. subtilis* are well-established, the specific mechanisms of their generation during the MFC's operational phase and across the germination cycle necessitate in-depth examination. Undertaking such studies is crucial for refining MFC designs to achieve optimal therapeutic outcomes, ensuring the elimination of pathogenic bacteria and facilitating wound repair.

4. CONCLUSIONS

This research presents a groundbreaking approach to wound care by introducing a bioelectrochemical system-based living wound dressing, using MFC technology. This innovative dressing incorporates nanoparticles-decorated *B. subtilis* endospores, which possess inherent antibacterial properties. The unique design of the dressing enables it to use nutrient-rich wound exudate to germinate the endospores, activating their metabolic processes. Upon activation, the dressing initiates electrical current generation, providing electrical stimulation therapy to infected wounds. This process is enhanced as the germinated *B. subtilis* detects pathogens, triggering the production of antibacterial agents. The incorporation of biosynthesized nanoparticles enhances the electron transfer efficiency, significantly boosting the electrical stimulation's therapeutic efficacy. This multifaceted antibacterial therapeutic strategy offers a novel and effective solution to the complex challenges of wound management. The MFC is engineered on a disposable, flexible, and porous paper substrate, making it exceptionally suitable for wearable wound dressing applications. The integration of a conductive hydrogel into the paper substrate significantly enhances the mechanical and biological performance of the MFC, offering improved comfort and efficacy. Comprehensive in vitro and ex vivo studies underscore the MFC dressing's capability for effective pathogen management. These investigations highlight the dressing's potent antibacterial mechanisms, showcasing its potential to significantly impact the overall performance and stability of the system in environments rich in pathogens. This work advances the field of wound care and opens new avenues for the development of bioelectrochemical systems in medical applications.

5. MATERIALS AND METHODS

5.1. *B. subtilis* Inoculum. The *Bacillus subtilis* strain 168, sourced from the American Type Culture Collection, was cultured in a Luria Broth (LB) medium under conditions of gentle agitation at 37 °C for 24 h. The proliferation of the *B. subtilis* culture was quantitatively assessed by measuring the optical density at a wavelength of 600 nm (OD_{600}). When the culture attained an OD_{600} value of 2.0, indicative of a specific cell density, the bacterial cells were systematically collected via centrifugation. Following collection, the cells underwent serial dilution to adjust their concentration for their designated roles in forthcoming experimental procedures. This careful preparation ensures the reproducibility and reliability of the bacterial samples for subsequent investigations, providing a standardized basis for exploring the bacterium's potential applications.

https://doi.org/10.1021/acsami.4c06303
ACS Appl. Mater. Interfaces 2024, 16, 36117−36130

5.2. Extracellular Biosynthesis of SnO_2 and CuO Nanoparticles. A designed experiment was conducted in which 1 mL of *B. subtilis* culture, exhibiting an optical density of 1.5 at 600 nm (OD_{600}), was resuspended in 7 mL of a fresh LB medium. This suspension was then enriched with 1 mg of tin(II) chloride ($SnCl_2$) and 0.5 mg of copper(II) chloride ($CuCl_2$), facilitating a complex biochemical interaction. The mixture was incubated overnight at 37 °C under anaerobic conditions, a critical step that induced the extracellular synthesis of nanoparticles while simultaneously prompting the bacterial cells to initiate sporulation, transitioning into endospores. Following incubation, the solution, now enriched with SnO_2 and CuO nanoparticles adhered to the endospores, heated at 60 °C for 30 min. This procedure eliminated remaining vegetative cells without compromising the integrity of the endospores or the attached nanoparticles. Subsequent centrifugation at 4000 rpm for 5 min helped collect the nanoparticle-decorated endospores. To achieve a high degree of purity and ensure the removal of any contaminants, the collected sample underwent four successive washes with deionized water. The successful synthesis of SnO_2 and CuO nanoparticles, intricately associated with the endospores, was verified through advanced analytical techniques, specifically SEM coupled with energy-dispersive X-ray spectroscopy (EDX). This process confirmed the formation of the desired nanoparticles and underscored the potential of this novel approach in synthesizing nanomaterials for a broad range of biotechnological applications.

5.3. Synthesis of Composite Hydrogel. The synthesis of an advanced hydrogel composite, integrating graphene (G0501, Tokyo Chemical Industry), sodium alginate (W201502, Sigma-Aldrich), and gelatin (G2500, Sigma-Aldrich), was executed using a hydrothermal method. Initially, solutions of sodium alginate (200 mg dissolved in 10 mL deionized water) and gelatin (500 mg in 10 mL deionized water) were prepared through rigorous stirring to achieve complete dissolution of each polymer. Following this, a 20-mL graphene suspension (2 mg/mL) was methodically blended with the sodium alginate solution, after which the gelatin solution was incrementally introduced to the mixture. To facilitate the formation of a stable, 3D polymeric network, 1 mL of glutaraldehyde (Sigma-Aldrich), serving as a cross-linking agent, was incorporated into the blend. This precursor mixture was subsequently subjected to a hydrothermal reaction within an autoclave, maintained at 180 °C for 18 h. The specific conditions of high temperature and pressure within the autoclave were instrumental in promoting the intermolecular interactions necessary for the development of the hydrogel matrix. After the treatment and subsequent cooling to room temperature, the hydrogel was washed three times with deionized water to eliminate any residual reactants, followed by a 24-h freeze-drying process to yield the final composite. Further functionalization of the hydrogel added 100 mg of the composite to a solution containing 2 mL of poly(3,4-ethylenedioxythiophene):polystyrenesulfonate (PEDOT:PSS, 1 wt %, Clevios PH1000, Heraeus) and 100 μL of dimethyl sulfoxide (DMSO, D8418-100 ML, Sigma-Aldrich), with the mixture being stirred for 1 h to ensure homogeneity. The incorporation of decorated endospores into the hydrogel matrix was achieved by introducing 50 μL of an endospore-containing solution into the composite, followed by stirring for 5 h to allow for adequate integration. Subsequently, 35 μL of this enriched hydrogel solution with the endospores was precisely deposited onto a designated anodic region, following the careful engineering and functional design of this composite hydrogel.

In the control experiment designed to assess the influence of sodium alginate and gelatin on the composite's properties, a simplified formulation was prepared using 100 mg of commercially sourced graphene powder. This graphene was directly integrated with 2 mL of a PEDOT:PSS solution, and 100 μL of DMSO to facilitate dispersion and improve the interaction between components. The mixture stirred thoroughly to ensure a uniform dispersion of the graphene particles within the PEDOT:PSS matrix. The subsequent experimental procedures were carefully replicated as per the original protocol involving sodium alginate and gelatin-based hydrogels.

5.4. Fabrication of Paper-Based MFC Wound Dressings. In this advanced material fabrication process, a precise and innovative method was employed to create a paper-based MFC. We delineated specific zones in the device for the anode, membrane, and cathode on a substrate of Whatman 3 MM CHR filter paper by using a wax printer (Xerox Phaser, ColorQube 8570). This technique involved the application of a hydrophobic wax pattern to both sides of the filter paper, ensuring the creation of well-defined and isolated sections critical for the functionality of the MFC system. Following the wax patterning, the filter paper was heated at 150 °C for 30 s. This step is crucial for ensuring the complete penetration and solidification of the wax into the paper's fibrous structure, thereby effectively creating hydrophobic barriers that prevent cross-contamination between different functional areas of the device. For the anodic region, a carefully measured volume of 35 μL from the hydrogel solution enriched with nanoparticle-decorated endospores was precisely dispensed onto the designated area, establishing the bioanode. In a parallel preparation for the cathodic section, a mixture comprising a 200 mg of silver oxide (Ag_2O; 11407-14, Alfa Aesar), 2 mL of PEDOT:PSS solution and 100 μL of DMSO was prepared. This mixture was stirred for 1 h to achieve a homogeneous 15 μL solution, which was then applied to the predetermined cathodic region, forming the biocathode. To complete the circuit and facilitate electrical connectivity within the system, nickel spray was employed to establish conductive links on the anodic and cathodic sections.

5.5. Fabrication of Infected Wound Models. In our in vitro study, we engineered a skin-analogous platform with a focus on accurately replicating the conductivity of individual skin layers. Agar served as the primary substrate because of its versatility and biocompatibility. To endow the agar substrate with electrical conductivity, a series of experiments were conducted to identify the optimal combination of materials. The process commenced with the dissolution of 258 mg of polypyrrole (Sigma-Aldrich) into 10 mL of deionized water, followed by continuous stirring for 1 h to ensure complete dissolution. Subsequently, 100 mg of agar was gradually introduced into the polypyrrole solution. Continuous stirring facilitated the achievement of a uniform mixture, after which, poly(vinyl alcohol) (PVA, Sigma-Aldrich) at a concentration of 10% was added as a binding agent to enhance the structural integrity of the composite. The mixture was then stirred for an additional 2 h to ensure thorough integration of all components. To tailor the conductivity of the mixture to resemble more closely that of human skin, 80 mg of sodium chloride and 70 mg of calcium chloride were incorporated. The solution's temperature was elevated to 110 °C for 30 min to facilitate the complete interaction of the components. Upon completion of this process, the agar-polypyrrole solution was poured into a Petri dish and allowed to cool to room temperature, solidifying into a conductive hydrogel. The achieved resistance level closely aligns with that of the human epidermis, underscoring the platform's capability to serve as a physiologically accurate skin model. Through experimentation with the composition of the hydrogel, particularly by modifying the polypyrrole-to-agar ratio, we were able to induce significant changes in the electrical conductivity of the agar substrate. Specifically, a 1:1 ratio of polypyrrole to agar yielded a resistance of approximately 12 kΩ, which parallels the electrical resistance characteristic of the human epidermis. Enhancing the ratio to 2:1 markedly increased the conductivity, reducing the resistance to 5 kΩ, thereby emulating the electrical properties of the deeper skin layer, the dermis. This nuanced control over the hydrogel's electrical properties via adjustment of the polypyrrole and agar ratios facilitates a highly versatile modeling approach. It allows for the precise simulation of different skin layers' electrical characteristics, making it an invaluable tool for investigating the effect of various treatments on skin-like materials. Furthermore, this methodological flexibility opens avenues for exploring the effects of altered electrical properties on skin condition models, paving the way for innovative dermatological research and potential therapeutic applications.

5.6. Simulated Wound Exudate. We formulated a synthetic wound exudate designed to mimic the complex composition of fluid from human wounds, enhancing the realism of our experimental

https://doi.org/10.1021/acsami.4c06303
ACS Appl. Mater. Interfaces 2024, 16, 36117−36130

model. This artificial exudate comprises 500 mg of sodium chloride, 320 mg of sodium hydrogen carbonate, 250 mg of potassium chloride, 250 mg of calcium chloride, and 200 mg of glucose, supplemented with 3.0 g of bovine albumin to replicate the protein-rich environment of natural wound fluid. The entire mixture was solubilized in 100 mL of deionized water, ensuring a homogeneous solution that closely resembles the electrolyte and nutrient profile of human wound exudate. The inclusion of glucose and albumin in the artificial exudate serves a dual purpose. Primarily, it acts as a critical nutrient source, facilitating the germination of Bacillus endospores. This feature is pivotal in our studies, as the ability of *Bacillus* endospores to germinate in response to the glucose concentration closely simulates the microbial dynamics observed in actual wound healing scenarios. By replicating these conditions, our model provides invaluable insights into the behavior of microorganisms within wound environments and the potential therapeutic interventions to promote healing and prevent infection.

5.7. Ex Vivo Evaluation. For our study, porcine skin samples were prepared by first selecting frozen skin and then excising sections of approximately 20 mm^2, with a thickness ranging from 8.0 to 10 mm. The removal of the epidermal layer and the creation of a standardized, full-thickness wound at the center of each sample were achieved using a 4 mm diameter biopsy punch and a scalpel. This step was critical for simulating a wound environment conducive to the introduction of planktonic pathogenic bacteria. Following the initial preparation, these skin explants were submerged in a PBS solution and maintained in this condition for the duration of the experimental protocols. The MFC was then meticulously applied to the surface of each prepared skin sample. To ensure a robust and stable attachment of the MFC to the porcine skin, we used a transdermal adhesive patch, specifically designed for medical applications, to secure the device in place. Throughout the experiment, to simulate the dynamic nature of wound healing and infection management, 100 μL of synthetic wound exudate were periodically introduced directly into the wound site at 6 h intervals. This procedure mimicked the continuous fluid exchange found in real wound scenarios and provided a consistent medium for testing the efficacy of the MFC in a controlled, yet realistic, biological environment.

5.8. Electrochemical Experiments. Electrochemical analyses, specifically CV and EIS, were performed using a Squidstat Plus potentiostat from Admiral Instruments. These measurements evaluated the anodic performance in the presence of various biocatalysts within a precisely configured three-electrode electrochemical cell. This cell's configuration included a platinum foil counter electrode and an Ag/AgCl electrode submerged in saturated KCl, serving as the reference electrode, to ensure accurate and reliable measurements. For the CV assessments, scans were executed at a sweep rate of 100 mV/s across a potential range of −0.8 to 1.3 V. This wide voltage window allowed for a comprehensive analysis of the electrochemical behavior and performance of the biocatalysts under investigation. Meanwhile, the EIS measurements were conducted with an excitation voltage set at 0.5 V, exploring a broad frequency spectrum from 0.1 Hz to 100 kHz. This approach facilitated a detailed examination of the charge transfer processes and electrochemical kinetics associated with the biocatalyst−anode interface, providing invaluable insights into the system's overall efficiency and potential mechanisms of action.

5.9. Swelling and Water Retention Ratio Examination. To rigorously analyze the swelling kinetics of the composite hydrogel, we employed a methodical approach by immersing the samples in a PBS solution. The mass of the hydrogel samples was measured at specific intervals, allowing for precise monitoring until a saturation point was reached. This saturation point is characterized by the cessation of additional mass uptake by the hydrogel, indicating equilibrium between the hydrogel and the surrounding PBS solution. The swelling ratio, a key parameter in this study, was calculated by dividing the mass of PBS absorbed by the hydrogel by its initial dry mass, providing a quantitative measure of the hydrogel's capacity to absorb and retain liquid.

Furthermore, the water retention ratio (WRR) was used as a critical metric to assess the water retention capabilities of the materials under study. The WRR calculation involved determining the amount of water retained by the material. This experiment was conducted by saturating the specified material with the PBS buffer and subsequently measuring the retained water content over a designated period. This measure is instrumental in evaluating the material's effectiveness in maintaining moisture, a crucial factor for applications in wound healing and other biomedical fields where hydration plays a pivotal role in functionality.

5.10. Statistical Analysis. Experimental data presented in this work were derived from at least three identical experiments. Results are expressed as the mean ± standard error of these replicates.

■ ASSOCIATED CONTENT

Supporting Information

The Supporting Information is available free of charge at https://pubs.acs.org/doi/10.1021/acsami.4c06303.

The diameters of inhibition zones measured against three pathogens (*P. aeruginosa*, *E. coli*, and *S. aureus*), illustrating the antibacterial efficacy of *B. subtilis*; results from disk diffusion tests conducted on *B. subtilis* that have been enhanced with both SnO_2 and CuO nanoparticles; SEM images depicting *Bacillus subtilis* cells embedded within a three-dimensional hydrogel network; changes in the concentration of *E. coli*, *P. aeruginosa*, and *S. aureus* measured at OD_{600} with various samples; swelling ratio and WRR of the composite hydrogel versus graphene only; SEM image of pathogenic *P. aeruginosa* prior to damage inflicted by nanoparticle-decorated *Bacillus subtilis*; resistance optimization through numerous iterations of material combinations; SEM images of the simulated epidermis and dermis (PDF)

■ AUTHOR INFORMATION

Corresponding Author

Seokheun Choi − *Bioelectronics & Microsystems Laboratory, Department of Electrical & Computer Engineering, State University of New York at Binghamton, Binghamton, New York 13902, United States; Center for Research in Advanced Sensing Technologies & Environmental Sustainability, State University of New York at Binghamton, Binghamton, New York 13902, United States;* orcid.org/0000-0003-1097-2391; Email: sechoi@binghamton.edu

Authors

Maryam Rezaie − *Bioelectronics & Microsystems Laboratory, Department of Electrical & Computer Engineering, State University of New York at Binghamton, Binghamton, New York 13902, United States*

Zahra Rafiee − *Bioelectronics & Microsystems Laboratory, Department of Electrical & Computer Engineering, State University of New York at Binghamton, Binghamton, New York 13902, United States*

Complete contact information is available at: https://pubs.acs.org/10.1021/acsami.4c06303

Author Contributions

M. Rezaie contributed to analysis, investigation, and methodology. Z. Rafiee contributed to analysis, and investigation. S. Choi contributed to visualization, funding acquisition, project

https://doi.org/10.1021/acsami.4c06303
ACS Appl. Mater. Interfaces 2024, 16, 36117−36130

administration, supervision, writing-original draft, and writing-review and editing.

Notes

The authors declare no competing financial interest.

■ ACKNOWLEDGMENTS

This study received funding from the National Science Foundation (grant nos 2246975 and 2100757). We thank the Analytical and Diagnostic Laboratory at SUNY-Binghamton for granting access to their facilities. In drafting this manuscript, we used ChatGPT to identify and correct grammatical errors. After this assistance, we meticulously reviewed and revised the document as needed. The authors bear full responsibility for the content of this publication.

■ REFERENCES

(1) He, X.; Yang, S.; Liu, C.; Xu, T.; Zhang, X. Integrated wound recognition in bandages for intelligent treatment. *Adv. Healthcare Mater.* **2020**, *9*, 2000941.
(2) Li, S.; Wang, X.; Yan, Z.; Wang, T.; Chen, Z.; Song, H.; Zheng, Y. Microneedle patches with antimicrobial and immunomodulating properties for infected wound healing. *Adv. Sci.* **2023**, *10*, 2300576.
(3) Byrd, A. L.; Belkaid, Y.; Segre, J. A. The human skin microbiome. *Nat. Rev. Microbiol.* **2018**, *16*, 143−155.
(4) Dwyer, L. R.; Scharschmidt, T. C. Early life host-microbe interactions in skin. *Cell Host Microbe* **2022**, *30*, 684−695.
(5) Grice, E. A.; Kong, H. H.; Conlan, S.; Deming, C. B.; Davis, J.; Young, A. C.; Bouffard, G. G.; Blakesley, R. W.; Murray, P. R.; Green, E. D.; Turner, M. L.; Segre, J. A.; NISC Comparative Sequencing Program. Topographical and temporal diversity of the human skin microbiome. *Science* **2009**, *324*, 1190−1192.
(6) Brown, E. D.; Wright, G. D. Antibacterial drug discovery in the resistance era. *Nature* **2016**, *529*, 336−343.
(7) Shi, L.; Liu, X.; Wang, W.; Jiang, L.; Wang, S. A self-pumping dressing for draining excessive biofluid around wounds. *Adv. Mater.* **2019**, *31*, 1804187.
(8) Gao, Y.; Elhadad, A.; Choi, S. Janus Paper-based Wound Dressings for Effective Exudate Absorption and Antibiotic Delivery. *Adv. Eng. Mater.* **2024**, *26*, 2301422.
(9) Vivcharenko, V.; Trzaskowska, M.; Przekora, A. Wound dressing modifications for accelerated healing of infected wounds. *Mol. Sci.* **2023**, *24*, 7193.
(10) Negut, I.; Grumezescu, V.; Grumezescu, A. M. Treatment strategies for infected wounds. *Molecules* **2018**, *23*, 2392.
(11) Darvishi, S.; Tavakolik, S.; Kharaziha, M.; Girault, H. H.; Kaminski, C. F.; Mela, I. Advances in the sensing and treatment of wound biofilms. *Angew. Chem., Int. Ed.* **2022**, *61*, No. e202112218.
(12) Diban, F.; Di Lodovico, S.; Di Fermo, P.; D'Ercole, S.; D'Arcangelo, S.; Di Giulio, M.; Cellini, L. Biofilms in Chronic Wound Infections: Innovative Antimicrobial Approaches Using the In Vitro Lubbock Chronic Wound Biofilm Model. *Int. J. Mol. Sci.* **2023**, *24*, 1004.
(13) Ghomi, E. R.; Niaze, M.; Ramakrishna, S. The evolution of wound dressings: From traditional to smart dressings. *Polym. Adv. Technol.* **2023**, *34*, 520−530.
(14) Yousefian, F.; Hesari, R.; Jensen, T.; Obagi, S.; Rgeai, A.; Damiani, G.; Bunick, C. G.; Grada, A. Antimicrobial wound dressings: a concise review for clinicians. *Antibiotics* **2023**, *12*, 1434.
(15) Di Domizio, J.; Belkhodja, C.; Chenuet, P.; Fries, A.; Murray, T.; Mondéjar, P. M.; Demaria, O.; Conrad, C.; Homey, B.; Werner, S.; Speiser, D. E.; Ryffel, B.; Gilliet, M. The commensal skin microbiota triggers type I IFN-dependent innate repair responses in injured skin. *Nat. Immunol.* **2020**, *21*, 1034−1045.
(16) Su, S.; He, J.; Wang, C.; Gao, F.; Zhong, D.; Lei, P. A New Dressing System Reduces the Number of Dressing Changes in the Primary Total Knee Arthroplasty: A Randomized Controlled Trial. *Front. Surg.* **2022**, *9*, 800850.
(17) O'Toole, P. W.; Marchesi, J. R.; Hill, C. Next-generation probiotics: the spectrum from probiotics to live biotherapeutics. *Nat. Microbiol.* **2017**, *2*, 17057.
(18) Ming, Z.; Han, L.; Bao, M.; Zhu, H.; Qiang, S.; Xue, S.; Liu, W. Living bacterial hydrogels for accelerated infected wound healing. *Adv. Sci.* **2021**, *8*, 2102545.
(19) Wang, W.; Ummartyotin, S.; Narain, R. Advances and challenges on hydrogels for wound dressing. *Curr. Opin. Biomed. Eng.* **2023**, *26*, 100443.
(20) Falagas, M. E.; Betsi, G. I.; Tokas, T.; Athanasiou, S. Probiotics for prevention of recurrent urinary tract infections in women: a review of the evidence from microbiological and clinical studies. *Drugs* **2006**, *66*, 1253−1261.
(21) Lufton, M.; Bustan, O.; Eylon, B.; Shtifman-Segal, E.; Croitoru-Sadger, T.; Shagan, A.; Shabtay-Orbach, A.; Corem-Salkmon, E.; Berman, J.; Nyska, A.; Mizrahi, B. Living Bacteria in Thermoresponsive Gel for Treating Fungal Infections. *Adv. Funct. Mater.* **2018**, *28*, 1801581.
(22) Chen, G.; Wang, F.; Zhang, X.; Shang, Y.; Zhao, Y. Living microecological hydrogels for wound healing. *Sci. Adv.* **2023**, *9*, No. eadg3478.
(23) Qona'ah, A.; Suliyanti, M. M.; Hidayanto, E.; Khumaeni, A. Characteristics of copper oxide and tin oxide nanoparticles produced by using pulsed laser ablation method and their application as an antibacterial agent. *Results Chem.* **2023**, *6*, 101042.
(24) Liu, L.; Choi, S. Enhanced Biophotoelectricity Generation in Cyanobacterial Biophotovoltaics with Intracellularly Biosynthesized Gold Nanoparticles. *J. Power Sources* **2021**, *506*, 230251.
(25) Rezaie, M.; Rafiee, Z.; Choi, S. A Transient Spore-forming Microbial Fuel Cell with Extracellularly Biosynthesized Tin Oxide Nanoparticles for Powering Disposable and Green Papertronics. *Adv. Sustainable Syst.* **2024**, *8*, 2300357.
(26) Kulkarni, D.; Sherkar, R.; Shirsathe, C.; Sonwane, R.; Varpe, N.; Shelke, S.; More, M. P.; Pardeshi, S. R.; Dhaneshwar, G.; Junnuthula, V.; Dyawanapelly, S. Biofabrication of nanoparticles: sources, synthesis, and biomedical applications. *Front. Bioeng. Biotechnol.* **2023**, *11*, 1159193.
(27) Jalili, P.; Ala, A.; Nazari, P.; Jalili, B.; Ganji, D. D. A comprehensive review of microbial fuel cells considering materials, methods, structures, and microorganisms. *Heliyon* **2024**, *10*, No. e25439.
(28) Lovley, D. R. Electromicrobiology. *Annu. Rev. Microbiol.* **2012**, *66*, 391−409.
(29) Logan, B. E. Scaling up microbial fuel cells and other bioelectrochemical systems. *Appl. Microbiol. Biotechnol.* **2010**, *85*, 1665−1671.
(30) Dewan, A.; Beyenal, H.; Lewandowski, Z. Scaling up microbial fuel cells. *Environ. Sci. Technol.* **2008**, *42*, 7643−7648.
(31) Schröder, U. Discover the possibilities: Microbial bioelectrochemical systems and the revival of a 100-year-old discovery. *J. Solid State Electrochem.* **2011**, *15*, 1481−1486.
(32) Arends, J. B. A.; Verstrete, W. 100 years of microbial electricity production: three concepts for the future. *Microb. Biotechnol.* **2012**, *5*, 333−346.
(33) Choi, S. Biofuel cells and Biobatteries: Misconceptions, Opportunities, and Challenges. *Batteries* **2023**, *9*, 119.
(34) Gao, Y.; Mohammadifar, M.; Choi, S. From microbial fuel cells to Biobatteries: Moving toward on-demand micro-power generation for Small-scale Single-Use Applications. *Adv. Mater. Technol.* **2019**, *4*, 1970039.
(35) Choi, S. Electrogenic Bacteria Promise New Opportunities for Powering, Sensing, and Synthesizing. *Small* **2022**, *18*, 2107902.
(36) Qian, F.; Baum, M.; Gu, Q.; Morse, D. E. A 1.5 μL microbial fuel cell for on-chip bioelectricity generation. *Lab Chip* **2009**, *9*, 3076.
(37) Greenman, J.; Mendis, A.; You, J.; Gajda, I.; Horsfield, I.; Ieropoulos, I. Microbial fuel cell based thermosensor for robotic applications. *Front. Robot. AI* **2021**, *8*, 558953.

https://doi.org/10.1021/acsami.4c06303
ACS Appl. Mater. Interfaces 2024, 16, 36117−36130

(38) Elhadad, A.; Gao, Y.; Choi, S. Integrating Renewable Microbial Fuel Cells in Dual In-Line Package for Chip-on-Board-Circuits. *Adv. Mater. Technol.* **2023**, *8*, 2301035.
(39) Elhadad, A.; Choi, S. Powering the Internet of Things in Aquatic Environments: Solar Energy Harvesting Through a Buoyant Biosolar Cell Array. *J. Power Sources* **2023**, *581*, 233501.
(40) Light, S. H.; Su, L.; Rivera-Lugo, R.; Cornejo, J. A.; Louie, A.; Iavarone, A. T.; Ajo-Franklin, C. M.; Portnoy, D. A. A flavin-based extracellular electron transfer mechanism in diverse Gram-positive bacteria. *Nature* **2018**, *562*, 140−144.
(41) Landers, M.; Choi, S. Small-scale, Storable Paper Biobatteries Activated Via Human Bodily Fluids. *Nano Energy* **2022**, *97*, 107227.
(42) Tahernia, M.; Plotkin-Kaye, E.; Mohammadifar, M.; Gao, Y.; Oefelein, M.; Cook, L.; Choi, S. Characterization of Electrogenic Gut Bacteria. *ACS Omega* **2020**, *5*, 29439−29446.
(43) Mohammadifar, M.; Tahernia, M.; Yang, J. H.; Koh, A.; Choi, S. Biopower-on-Skin: Electricity generation from sweat-eating bacteria for self-powered e-skins. *Nano Energy* **2020**, *75*, 104994.
(44) Ryu, J.; Choi, S. Bioelectricity Production from Sweat-Activated Germination of Bacterial Endospores. *Biosens. Bioelectron.* **2021**, *186*, 113293.
(45) Ryu, J.; Landers, M.; Choi, S. A Sweat-Activated, Wearable Microbial Fuel Cell for Long-term, On-demand Power Generation. *Biosens. Bioelectron.* **2022**, *205*, 114128.
(46) Gao, Y.; Rezaie, M.; Choi, S. A wearable, disposable paper-based self-charging power system integrating sweat-driven microbial energy harvesting and energy storage devices. *Nano Energy* **2022**, *104*, 107923.
(47) Savitskaya, I. S.; Shokatayeva, D. H.; Kistaubayeva, A. S.; Ignatova, L. V.; Digel, I. E. Antimicrobial and wound dealing properties of a bacterial cellulose based material containing *B. subtilis* cells. *Heliyon* **2019**, *5*, No. e02592.
(48) Yan, L.; Liu, G.; Zhao, B.; Pang, B.; Wu, W.; Ai, C.; Zhao, X.; Wang, X.; Jiang, C.; Shao, D.; Liu, Q.; Li, M.; Wang, L.; Shi, J. Novel biomedical functions of surfactin A from *Bacillus subtilis* in wound healing promotion and scar inhibition. *J. Agric. Food Chem.* **2020**, *68*, 6987−6997.
(49) Stein, T. *Bacillus subtilis* antibiotics: structures, syntheses and specific functions. *Mol. Microbiol.* **2005**, *56*, 845−857.
(50) Maan, H.; Itkin, M.; Malitsky, S.; Friedman, J.; Kolodkin-Gal, I. Resolving the conflict between antibiotic production and rapid growth by recognition of peptidoglycan of susceptible competitors. *Nat. Commun.* **2022**, *13*, 431.
(51) Tirono, M.; Hananto, F. S.; Abtokhi, A. Pulse Voltage Electrical Stimulation for Bacterial Inactivation and Wound Healing in Mice with Diabetes. *Avicenna J. Med. Biotechnol.* **2022**, *14*, 95.
(52) Tasai, H.; Lin, Y.; Huang, K.; Yang, C.; Chou, C.; Chao, L. Reduction of Viral and Bacterial Activity by Using a Self-Powered Variable-Frequency Electrical Stimulation Device. *Micromachines* **2023**, *14*, 282.
(53) Asadi, M. R.; Torkaman, G. Bacterial inhibition by electrical stimulation. *Adv. Wound Care* **2014**, *3*, 91−97.
(54) Mohammadifar, M.; Zhang, J.; Yazgan, I.; Sadik, O.; Choi, S. Power-on-paper: Origami-inspired Fabrication of 3-D Microbial Fuel Cells. *Renew. Energy* **2018**, *118*, 695−700.
(55) Gao, Y.; Choi, S. Merging Electric Bacteria with Paper. *Adv. Mater. Technol.* **2018**, *3*, 1800118.
(56) Abe, Y.; Nishizawa, M. Electrical aspects of skin as a pathway to engineering skin devices. *APL Bioeng.* **2021**, *5*, 041509.
(57) Huang, M.; Hull, C. M. Sporulation: how to survive on planet Earth and beyond. *Curr. Genet.* **2017**, *63*, 831−838.
(58) Mazur, F.; Tjandra, A. D.; Zhou, Y.; Gao, Y.; Chandrawati, R. Paper-based sensors for bacteria detection. *Nat. Rev. Bioeng.* **2023**, *1*, 180−192.
(59) Xu, C.; Akakuru, O. U.; Ma, X.; Zheng, J.; Zheng, J.; Wu, A. Nanoparticle-Based Wound Dressing: Recent Progress in the Detection and Therapy of Bacterial Infections. *Bioconjugate Chem.* **2020**, *31*, 1708−1723.
(60) Deng, X.; Gould, M.; Ali, M. A. A review of current advancements for wound healing: Biomaterial applications and medical devices. *J. Biomed. Mater. Res.* **2022**, *110*, 2542−2573.
(61) Logan, B. E. Exoelectrogenic bacteria that power microbial fuel cells. *Nat. Rev. Microbiol.* **2009**, *7*, 375−381.
(62) Garnett, J. P.; Kalsi, K. K.; Sobotta, M.; Bearham, J.; Carr, G.; Powell, J.; Brodlie, M.; Ward, C.; Tarran, R.; Baines, D. L. Hyperglycaemia and Pseudomonas aeruginosa acidify cystic fibrosis airway surface liquid by elevating epithelial monocarboxylate transporter 2 dependent lactate-H+ secretion. *Sci. Rep.* **2016**, *6*, 37955.
(63) Luo, R.; Dai, J.; Zhang, J.; Li, Z. Accelerated Skin Wound Healing by Electrical Stimulation. *Adv. Healthcare Mater.* **2021**, *10*, 2100557.

https://doi.org/10.1021/acsami.4c06303
ACS Appl. Mater. Interfaces 2024, 16, 36117−36130